XML-IS

Our reference: ISATRA 1602 P-authorquery-vx

**AUTHOR QUERY FORM**

| | | |
|---|---|---|
| ELSEVIER | **Journal: ISATRA**<br><br>**Article Number: 1602** | **Please e-mail or fax your responses and any corrections to:**<br><br>**E-mail: corrections.essd@elsevier.macipd.com**<br><br>**Fax: +44 1392 285878** |

Dear Author,

Please check your proof carefully and mark all corrections at the appropriate place in the proof (e.g., by using on-screen annotation in the PDF file) or compile them in a separate list. Note: if you opt to annotate the file with software other than Adobe Reader then please also highlight the appropriate place in the PDF file. To ensure fast publication of your paper please return your corrections within 48 hours.

For correction or revision of any artwork, please consult http://www.elsevier.com/artworkinstructions.

Any queries or remarks that have arisen during the processing of your manuscript are listed below and highlighted by flags in the proof. Click on the Q link to go to the location in the proof.

| Location in article | Query / Remark: click on the Q link to go<br>Please insert your reply or correction at the corresponding line in the proof |
|---|---|
| Q1 | Please confirm that given names and surnames have been identified correctly and are presented in the desired order. |
| Q2 | Please check the telephone number of the corresponding author, and correct if necessary. |

Thank you for your assistance.

Please check this box or indicate your approval if you have no corrections to make to the PDF file ☑

ISA Transactions ▮ (▮▮▮▮) ▮▮▮–▮▮▮

Contents lists available at SciVerse ScienceDirect

ISA Transactions

journal homepage: www.elsevier.com/locate/isatrans

# Highlights



## Application of Laguerre based adaptive predictive control to Shape Memory Alloy (SMA) Actuator

Q1 S. Kannan [a], C. Giraud-Audine [b], E. Patoor [a]

[a] Laboratoire d'Etude des Microstructures et de Mécanique des Matériaux (LEM3)—CNRS, Arts et Métiers Paristech-Metz, 4 rue Augustin Fresnel, Metz 57078, France
[b] Laboratoire d'Electrotechnique et d'Electronique de Puissance (L2EP), Arts et Métiers Paristech-Lille, 8 Bd Louis XIV, Lille 59000, France

► A Laguerre adaptive predictive controller applied to linear SMA actuator is investigated. ► Stability is guaranteed if the prediction horizon respects some bounds. ► For a bounded modeling error, the steady state error is asymptotically stable. ► Experimental results obtained on two different actuators are thoroughly presented.



0019-0578/$ - see front matter © 2013 Published by Elsevier Ltd. on behalf of ISA.
http://dx.doi.org/10.1016/j.isatra.2013.02.004

ISA Transactions ▮ (▮▮▮▮) ▮▮▮–▮▮▮

Contents lists available at SciVerse ScienceDirect

ISA Transactions

journal homepage: www.elsevier.com/locate/isatrans

Practice Article

# Application of Laguerre based adaptive predictive control to Shape Memory Alloy (SMA) Actuator

Q1 S. Kannan[a], C. Giraud-Audine[b,*], E. Patoor[a]

[a] Laboratoire d'Etude des Microstructures et de Mécanique des Matériaux (LEM3)—CNRS, Arts et Métiers Paristech-Metz, 4 rue Augustin Fresnel, Metz 57078, France
[b] Laboratoire d'Electrotechnique et d'Electronique de Puissance (L2EP), Arts et Métiers Paristech-Lille, 8 Bd Louis XIV, Lille 59000, France

ARTICLE INFO

*Article history:*
Received 21 September 2011
Received in revised form
15 February 2013
Accepted 25 February 2013
This paper was recommended for publication by Dr. Jeff Pieper.

*Keywords:*
Laguerre functions
Adaptive control
Shape Memory Alloy actuator

ABSTRACT

This paper discusses the use of an existing adaptive predictive controller to control some Shape Memory Alloy (SMA) linear actuators. The model consists in a truncated linear combination of Laguerre filters identified online. The controller stability is studied in details. It is proven that the tracking error is asymptotically stable under some conditions on the modelling error. Moreover, the tracking error converge toward zero for step references, even if the identified model is inaccurate. Experimental results obtained on two different kind of actuator validate the proposed control. They also show that it is robust with regard to input constraints.





## 1. Introduction

Adaptive materials like Shape Memory Alloy (SMA) exhibit thermo-mechanical properties due to phase transition. This provides large strains, but it also induces a strong hysteretic behavior [1] changing with the aging of the material [2]. This hinders the development of SMA actuators which are commercially mostly limited to bistable-type applications, although many actuators have been proposed [3]. For more demanding applications such as positioning, control becomes necessary.

Similar problems can be found in the case of piezoelectric or magnetostrictive devices. In the literature, a usual approach to address the problem is to identify the hysteresis, then use an inverse model as a feed-forward compensation. A feedback loop is also necessary to handle the dynamic and compensate the modeling errors [4,5].

SMA, on the other hand belong to the class of Wiener model (as discussed in Section 2). Using an inverse of the hysteresis for a feed-forward compensation would only be efficient during steady state, hence other approaches have been proposed.

Physical models provide insight of the phenomena in the material. Unfortunately, they are often non-linear in the parameters and thus online identification is difficult. For instance, Benzaoui and Lexcellent [6] proposed a feedback linearization based on such a model but fifteen parameters must be identified off-line. Elahinia [7] proposed a simpler model requiring fewer off-line identification. Based on the model, an extended Kalman filter is used to observe temperature and stress in the material. A sliding mode controller is then used to control the device.

Alternatively, hysteresis can be modelled using operators with local memory triggered by the input and its variation. Such elementary operators – called hysterons – are the Preisach [4,5], Krasnosel'skii–Pokrovski (KP) [8] and Prandtl–Ishlinskii (PI) [9] operators. Combining each individual responses results in a non-local memory. Such models are exactly or approximately invertible [8–10]. One drawback is the necessity to know a weighting function associated to the hysterons and the tracking of their states which must be done on-line [11]. For instance, Webb and Lagoudas [8] used a KP model to identify the inverse hysteresis of an SMA which was used for a feed-forward compensation to generate a linearized reference. The control was realized using a gradient adaptive algorithm.

Artificial neural networks have also been proposed to address the problem. In [12], they are used to learn an input/output mapping corresponding to the inverse hysteresis. It is then used as a feedforward compensator. The loop is closed using a proportional integral controller. In [13], a neural network is used to approximate the resistance of the wire as a function of strain to realize a sensorless control. A proportional derivative controller is then used to compensate the error between the desired output and the predicted output. The later is obtained by the neural network based on the resistance measure. The drawbacks of

Q2 * Corresponding author. Tel.: +33 320621561.
*E-mail address:* christophe.giraud-audine@ensam.eu (C. Giraud-Audine).

0019-0578/$ - see front matter © 2013 Published by Elsevier Ltd. on behalf of ISA.
http://dx.doi.org/10.1016/j.isatra.2013.02.004

neural networks are the arbitrary choice of the structure and their training.

The cornerstone of the previous approaches is to model the internal state of the material either explicitly (physical models) or approximately (hysteresis model or neural networks). The price of this knowledge is the heavy computations involved and often a difficult identification. This is a serious limitation in practice where material properties vary due to manufacturing dispersion, and will evolve during the lifetime of the actuator.

As an alternative, in this paper, the system transfer function is updated on-line, and based on it the controller is tuned. The expected benefit of this simple model is to alleviate the computational effort. To do so, the order of the model should be low, hence the use of orthonormal basis functions to approximate the actual system dynamic. It is also necessary to keep the controller simple. Here, the predictive controller proposed by Zervos et al. is implemented [14]. The main contribution of this paper is to investigate some new properties of this controller: conditions of stability are established, and more importantly it is proved that the tracking error is asymptotically stable under certain conditions. When these requirements are met, it will converge to zero for step references. This motivates the use of this controller for SMA actuators where the non-linearity can induce bias in the identified parameters.

The outline of the paper is the following. In Section 2, based on the thermal behavior of SMA actuators, the use Laguerre filters is discussed. Since this model is to be adapted on-line, a directional forgetting recursive identification algorithm is introduced. Section 3 focuses on the adaptive predictive control using the Laguerre model. Stability conditions and convergence of the tracking error are studied. An experimental evaluation is presented in Section 4. The role of the main parameters of the controller is discussed. To this end, the controller is tested on two different actuators. The first one, simply consists in a wire submitted to constant stress. The non-linearity then simplifies to an hysteresis between strain and temperature. The second is a push–pull or antagonist actuator, involving two wires. The stress, strain, temperature hysteresis of each wires combine resulting in a complex "pinched" hysteresis. In both cases, the controller works satisfactorily. Finally, Section 5 discusses the results.

## 2. Model

### 2.1. Non-linearities in SMA wires

The dynamic of SMA actuator can be divided into two distinct parts: the thermal and the material behaviors. In this work, a simplified model of the thermal exchange commonly encountered in literature [15,8,6] is used. First, the simple case of a SMA wire submitted to a constant stress heated using Joules effect. The wire geometry is cylindrical. The section, diameter and length are respectively denoted $S$, $D$ and $l$. Considering convection as the dominant heat exchange mechanism [8,15], the wire temperature $T$ is governed by:

$$\rho c S l \frac{dT}{dt} + h\pi D l T = \underbrace{\frac{\sigma S}{l} V^2}_{P} + P_{ex} + h\pi D l T_{ext} \tag{1}$$

where $\rho$, $c$, $h$, $\sigma$, denote the density, the specific heat capacity, the convection coefficient, and the conductivity respectively. The powers appearing at the right hand side of Eq. (1) terms are:

- the electric power expressed using the voltage $V$ applied to the wire;
- the phase transition exogeneous power ($P_{ex}$);
- the power exchanged with the surrounding air (supposed to have the constant temperature $T_{ext}$).

In the sequel, $P_{ex}$ and $T_{ext}$ will be modeled disturbances and $V$ is the input of the system.

From this equation, the time constant $\tau$ and the gain $G$ of the thermal model can be expressed as

$$\begin{cases} \tau = \dfrac{\rho c}{4h} D \\ G = \dfrac{\sigma}{4h} \dfrac{D}{l^2} \end{cases} \tag{2}$$

Note that when the wire actuated, its dimensions will change, and so will the above coefficients. The volume being constant during the phase transformation [1], the diameter is a function of strain. Neglecting variations of $h$, the variation of the time constant and the gain can be estimated. In practice, to limit fatigue of the material, strain is kept under 4%, hence the variation of the time constant is around 2%. Finally roughly estimating the conductivity variation ca 10% [15] yields a maximum variation of the gain of approximately 20%.

In practice, the effects of these variations are negligible compared to the effect of hysteresis induced by the phase transition. Hence, the system can be considered as a linear block followed by an hysteresis block $\Gamma$, i.e. a Wiener non-linear system with the squared voltage as input as represented in Fig. 1. The exogenous power $P_{ex}$ and the ambient temperature $T_{ext}$ are modelled as disturbances. Therefore, in this work, the system is considered as a linear time varying system to be identified. The presence of the first order system (modelling the thermal transient) indicates that the system is highly damped. The hysteresis modifies the gain and the transient, and more importantly will act as a variable time delay. To capture these features, the input–output model used to elaborate the control will be based on Laguerre functions.

### 2.2. Laguerre model

Orthonormal rational functions applied to the modelling of dynamical systems have received special attention due to their numerous properties [16,17]. These functions are intrinsically stable infinite impulse response (IIR) filters and form a complete orthonormal set. Thus, any causal asymptotically stable system can be decomposed as an infinite series of such rational functions. For highly damped systems, Laguerre functions are best suited as they provide the best approximation given the dominant time constant. This a priori knowledge take full advantage of the Laguerre functions approximation properties, by improving the convergence [16,18]. Moreover, these functions can model time delay systems because of their similarities with the Pad'e approximation.

The discrete Laguerre expansion of a system having the transfer function $G(z)$ is given by

$$G(z) = \sum_{i=1}^{\infty} c_i L_i(z) \tag{3}$$

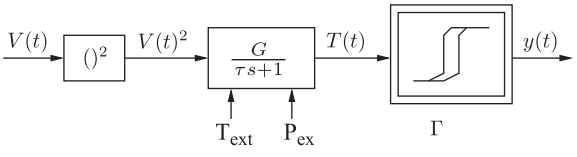


**Fig. 1.** Model structure for Shape Memory Alloy (SMA) Actuator.



Please cite this article as: Kannan S, et al. Application of Laguerre based adaptive predictive control to Shape Memory Alloy (SMA) Actuator. ISA Transactions (2013), http://dx.doi.org/10.1016/j.isatra.2013.02.004

where $c_i$ are called the weights of the Laguerre filter. The Laguerre function $L_i(z)$ can be calculated recursively. Introducing

$$L_0(z)=\frac{\sqrt{1-a^2}}{z-a}$$

$$L(z)=\frac{1-az}{z-a} \tag{4}$$

the $i$th Laguerre filter can be deduced from the previous order filter

$$L_i(z)=L(z)L_{i-1}(z) \tag{5}$$

This equation indicates that a Laguerre filter can be implemented using the classical so-called backbone structure.

Practically speaking, the model (3) has to be truncated. The choice of truncation order $N$ is related to the precision of the approximation not the order of the system. It can be reduced by a proper choice of the Laguerre pole $a$ [19]. Finally, Laguerre model complexity is reduced compared to ARX models [20].

The simplification can also be observed considering the state space form of the Laguerre filter. Using the outputs of the filters as the state variable $\mathbf{l}(t)=[l_0(t)\ \dots\ l_N(t)]^T$, a minimal state space realization is [21]

$$\begin{cases}\mathbf{l}(t+1)=\mathbf{A}\mathbf{l}(t)+\mathbf{B}u(t)\\ \hat{y}(t)=\hat{\mathbf{C}}^T(t)\mathbf{l}(t)\end{cases} \tag{6}$$

with

$$\mathbf{A}=\begin{bmatrix} a & 0 & \dots & 0\\ \beta & a & \ddots & 0\\ \vdots & \ddots & \ddots & 0\\ a^{N-2}\beta & \dots & \beta & a\end{bmatrix} \tag{7}$$

$$\mathbf{B}=\beta[1\ \ -a\ \ \dots\ \ (-a)^{N-1}]^T \tag{8}$$

where

$$\beta=\sqrt{1-a^2} \tag{9}$$

These matrices are entirely defined by the choice of the Laguerre pole $a$. $a\in\mathbb{R}$ must be in the unit circle for stability reasons and should be chosen close to the dominant dynamic of the system identified to reduce the truncation order $N$. From a practical point of view, it can be estimated from step responses, or in the case at hand using the expression of $\tau$ discussed in Section 2.1.

The output matrix collects all the model weights that must be identified

$$\hat{\mathbf{C}}(t)=[\hat{c}_0(t)\ \dots\ \hat{c}_{N-1}(t)]^T \tag{10}$$

Since the identification has to be performed on-line, an identification algorithm avoiding the loss of positiveness of the correlation matrix must be considered.

### 2.3. Identification algorithms

The output $\hat{y}(t)$ given by Eq. (6) is readily in regressor form with respect to $\mathbf{l}(t)$. Since the system is modelled as a linear time varying (LTV) system, an exponential forgetting algorithm must considered. To avoid the vanishing of the trace of the covariance matrix in closed loop, a directional forgetting RLS algorithm (DF-RLS) is implemented. Therefore, rather than systematically updating the covariance matrix, the old data are discarded only when they can be replaced by new ones. To do so, the update is done only in the directions which are excited [22]. The equations of the algorithm are

$$\hat{\mathbf{C}}(t)=\hat{\mathbf{C}}(t-1)+\mathbf{P}(t)\mathbf{l}(t)[y(t)-\mathbf{l}(t)^T\hat{\mathbf{C}}(t-1)] \tag{11}$$

where $\mathbf{P}(t)$ is the covariance matrix and $y(t)$ is the measured output at time step $t$. The covariance matrix $\mathbf{P}(t)$ is updated based on the following rule:

$$\mathbf{P}(t)=\overline{\mathbf{P}}(t-1)-\frac{\overline{\mathbf{P}}(t-1)\mathbf{l}(t)\mathbf{l}^T(t)\overline{\mathbf{P}}(t-1)}{1+\mathbf{l}^T(t)\overline{\mathbf{P}}(t-1)\mathbf{l}(t)} \tag{12}$$

$\overline{\mathbf{P}}(t-1)$ is the modified covariance matrix which is given by the following equations:

$$\overline{\mathbf{P}}(t-1)=\begin{cases}\mathbf{P}(t-1)+\dfrac{1-\lambda}{\lambda}\dfrac{\mathbf{l}(t)\mathbf{l}^T(t)}{\mathbf{l}^T(t)\mathbf{P}^{-1}(t-1)\mathbf{l}(t)} & \text{if } \|\mathbf{l}(t)\|\geq\eta\\ \mathbf{P}(t-1) & \text{if } \|\mathbf{l}(t)\|<\eta\end{cases} \tag{13}$$

The dead zone implemented using the $\eta$ threshold value guarantees that the matrix $R(t)$ remains bounded when the norm of the regressor is close to zero. Therefore, this value should usually be chosen accordingly to the noise level. In the case of the Laguerre model, the measurement noise is filtered by the low pass filter $L_0(z)$, thus the threshold $\eta$ should be chosen according to the filtered noise level of the sensors. $\lambda\in(0,1)$ is the forgetting factor which tunes the memory of the identification scheme. $\mathbf{P}^{-1}(t-1)$ in Eq. (13) is also calculated recursively using the information matrix

$$\mathbf{R}(t-1)=\mathbf{P}^{-1}(t-1)$$

$$\mathbf{R}(t)=[\mathbb{I}-\mathbf{M}(t)]\mathbf{R}(t-1)+\mathbf{l}(t)\mathbf{l}^T(t)$$

$$\mathbf{M}(t)=\begin{cases}(1-\lambda)\dfrac{\mathbf{R}(t-1)\mathbf{l}(t)\mathbf{l}^T(t)}{\mathbf{l}^T(t)\mathbf{R}(t-1)\mathbf{l}(t)} & \text{if } \|\mathbf{l}(t)\|\geq\eta\\ 0 & \text{if } \|\mathbf{l}(t)\|<\eta\end{cases} \tag{14}$$

The weights are initialized to zero, except for $\hat{c}_0$ to avoid singularity in the calculation of the controller's gains. The covariance matrix being the gain of the adaptation algorithm, it is initialized by $\mathbf{P}(0)=\delta^{-1}\mathbb{I}$ ($\mathbf{R}(0)=\delta\mathbb{I}$) with $\delta^{-1}\gg 1$ ($\mathbb{I}$ is the identity matrix of adequate dimensions). This choice results in a more responsive identification when the process starts. Finally, the choice of $\eta$ was not an issue during the experiments due to the excellent noise to signal ratio of the sensor employed.

## 3. Indirect adaptive predictive control

### 3.1. Predictor

Based the model given by Eq. (6), the following $H_p$ steps ahead predictor can be calculated by recursion

$$\hat{y}(t+H_p)=\hat{y}(t)+\hat{\mathbf{C}}^T(t)(\mathbf{A}^{H_p}-\mathbb{I})\mathbf{l}(t)+\hat{\mathbf{C}}^T(t)\left(\sum_{j=1}^{H_p}\mathbf{A}^{H_p-j}\mathbf{B}u(t+j-1)\right) \tag{15}$$

The predictor re-actualized at each step, thus in the previous equation $\hat{y}(t)$ is replaced by the available output measurement $y(t)$. This leads to

$$\hat{y}(t+H_p)=y(t)+\hat{\mathbf{C}}^T(t)(\mathbf{A}^{H_p}-\mathbb{I})\mathbf{l}(t)+\hat{\mathbf{C}}^T(t)\left(\sum_{j=1}^{H_p}\mathbf{A}^{H_p-j}\mathbf{B}u(t+j-1)\right) \tag{16}$$

Note that since the free response prediction is adjusted at each step according to the measurement and the current state of the model, a closed loop is implicitly implemented.



Please cite this article as: Kannan S, et al. Application of Laguerre based adaptive predictive control to Shape Memory Alloy (SMA) Actuator. ISA Transactions (2013), http://dx.doi.org/10.1016/j.isatra.2013.02.004

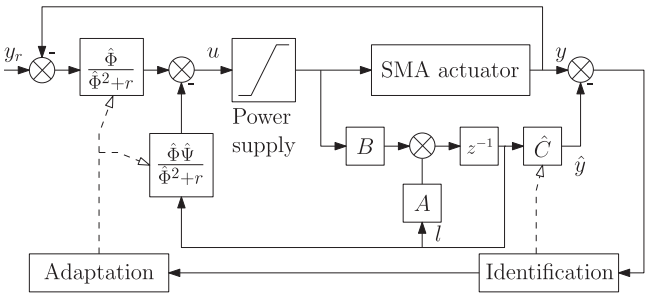


**Fig. 2.** Indirect adaptive predictive control based on the Laguerre model of the actuator.

### 3.2. Controller

The controller proposed in [23] is implemented. It calculates the input at time $t$ under the assumption that $u(t+j)=u(t)$ for $j\in\{1\dots H_p\}$. It is required that the system reaches a prescribed reference $y_r$ after $H_p$ steps. Setting $u(t)=u(t+1)=\cdots=u(t+H_p-1)$, and replacing $\hat{y}(t+H_p)$ by $y_r$ in the predictor given by Eq. (16), one can solve for $u(t)$

$$u(t)=\frac{[(y_r-y(t))-\hat{\boldsymbol{\Psi}}^T(t)\mathbf{l}(t)]}{\hat{\Phi}(t)} \tag{17}$$

where the gain $\hat{\Phi}(t)$ is defined by

$$\hat{\Phi}(t)=\hat{\mathbf{C}}^T(t)\mathbf{SB} \tag{18}$$

$\mathbf{S}$ being the matrix calculated by:

$$\mathbf{S}=\sum_{j=1}^{H_p}\mathbf{A}^{H_p-j} \tag{19}$$

and $\hat{\boldsymbol{\Psi}}(t)$ is a gains vector

$$\hat{\boldsymbol{\Psi}}^T(t)=\hat{\mathbf{C}}^T(t)(\mathbf{A}^{H_p}-\mathbb{I}) \tag{20}$$

As it will be explained in Section 4, some limitations regarding the currents through the wire have to be respected. In order to add more flexibility the following modified controller can be implemented:

$$u(t)=\frac{[(y_r(t)-y(t))-\hat{\boldsymbol{\Psi}}^T l(t)]\hat{\Phi}(t)}{\hat{\Phi}(t)^2+r} \tag{21}$$

where $r$ is a positive scalar weighting factor. Choosing $r=0$ leads to the controller (17). It can be shown that this controller minimizes the following performance index:

$$J=\sum_{i=1}^{H_p}(y_{ref}(t+i)-\hat{y}(t+i))^2+ru(t+i-1)^2 \tag{22}$$

thus, by varying $r$ a trade off between the control effort and the tracking error can be set.

The schematic of Fig. 2 sums up the control structure which can be considered as a combination of an output error feedback and a state feedback. The varying gains are updated according to the vector $\hat{\mathbf{C}}(t)$.

To justify this statement, let the $N$th order Laguerre model of the local linearization of the SMA actuator be given by

$$\begin{cases}\mathbf{l}_s(t+1)=\mathbf{A}l_s(t)+\mathbf{B}u(t)\\ y_s(t)=\mathbf{C}^T\mathbf{l}_s(t)\end{cases} \tag{23}$$

Since the Laguerre forms a complete set of orthonormal functions, such an approximation is always possible. $\mathbf{C}^T=[c_0,c_1,\dots c_{N-1}]$ are the actual values of the Laguerre system model. Owing to the orthonormal properties of the Laguerre function the coefficients $c_i$, $i\in\{0\dots N-1\}$ are not modified by the choice of the truncation order $N$, and the precision of the approximated model given by Eq. (23) can be reduced to an arbitrary value.

Subtracting Eqs. (6) to (23), the state error $\boldsymbol{\epsilon}(t)=\mathbf{l}_s(t)-\mathbf{l}(t)$ is given by

$$\boldsymbol{\epsilon}(t+1)=\mathbf{A}\boldsymbol{\epsilon}(t) \tag{24}$$

The state error is thus asymptotically stable, and will decrease to zero for any initial error on the state vector estimation, with a dynamic prescribed by the Laguerre poles.

### 3.3. Stability of the Laguerre model state

Assuming that $\boldsymbol{\epsilon}(t)$ has reached steady state, the closed loop system is

$$\mathbf{l}(t+1)=\left[\mathbf{A}-\frac{\hat{\Phi}(t)}{\hat{\Phi}(t)^2+r}\mathbf{B}\hat{\mathbf{C}}(t)^T\mathbf{A}^{H_p}\right]\mathbf{l}(t)+\mathbf{B}\frac{\hat{\Phi}(t)}{\hat{\Phi}(t)^2+r}y_r(t) \tag{25}$$

To study the stability the following lemma will be used [24]:

**Lemma 1.** *Consider the system*:

$$\mathbf{x}(t+1)=\mathcal{A}(t)\mathbf{x}(t)+\mathbf{v}(t) \tag{26}$$

1. *$\mathcal{A}(t)$ has finite coefficients for all $t$.*
2. *The eigen values of $\mathcal{A}(t)$ are inside the unit circle for all $t$.*
3. *$\|\mathcal{A}(t)-\mathcal{A}(t-1)\|\to 0$ for $t\to\infty$.*

*Then there exists a time $t$ such that*

$$\|\mathbf{x}(t+1)\|^2\le C_1+C_2\max_{0\le\tau\le t}\|\mathbf{v}(\tau)\|^2$$
$$\text{with } 0\le C_1,\ C_2<\infty \tag{27}$$

In the sequel, it will be assumed that the input signal is persistently exciting, hence the following properties [25] hold:

1. $\hat{\mathbf{C}}(t)$ and the identification error $\zeta(t)=y(t)-\hat{\mathbf{C}}(t)\mathbf{l}(t)$ are bounded.
2. There is a constant vector $\hat{\mathbf{C}}_\infty$ such that $\lim_{t\to\infty}\hat{\mathbf{C}}^T=\hat{\mathbf{C}}_\infty$.
3. $\hat{\mathbf{C}}(t+1)-\hat{\mathbf{C}}(t)$ belongs to $L_2$.

The case $r=0$ is first considered. From the definition of $\hat{\Phi}$ (Eq. (18)), and for a given $\hat{\mathbf{C}}(t)$, one can consider $\hat{\Phi}(H_p,t)$ the sequence of gains for different prediction horizons. The absolute increment between two successive values of the prediction horizon is

$$|\hat{\Phi}(H_p+1,t)-\hat{\Phi}(H_p,t)|=|\hat{\mathbf{C}}^T(t)\mathbf{A}^{H_p}\mathbf{B}|\le\|\hat{\mathbf{C}}^T(t)\|\|\mathbf{A}^{H_p}\|\|\mathbf{B}\| \tag{28}$$

where $\|\cdot\|$ denote the induced norm

$$\|\mathbf{x}\|=\|\mathbf{Q}\mathbf{x}\|_2\quad\text{with }\mathbf{Q}=\mathbf{UD} \tag{29}$$

with $\mathbf{U}$ a transformation matrix such that $\mathbf{U}^{-1}\mathbf{AU}=\mathbf{J_a}$ where $\mathbf{J_a}$ is the $N\times N$ Jordan block with value $a$ on its diagonal, and $\mathbf{D}$ is the diagonal matrix $\mathbf{D}=\text{diag}\{1,\xi,\dots,\xi^{N-1}\}$.

Applying the transformation defined by $\mathbf{Q}$ transforms $\mathbf{A}$ into $\mathbf{J}_\xi$ which is similar to $\mathbf{J_a}$ except that the ones above the diagonal are replaced by $\xi$ [25]. Hence, for this norm, the following result holds:

$$\|A^n\|^2\le(a+\xi)^{2n} \tag{30}$$

Using this norm, a bound for the increment of the gain with respect to $H_p$ is

$$|\hat{\Phi}(H_p+1,t)-\hat{\Phi}(H_p,t)|^2\le\|\hat{\mathbf{C}}(t)^T\|^2\|\mathbf{B}\|^2(a+\xi)^{2H_p} \tag{31}$$

Choosing $\xi$ such that $|\xi|<1-|a|$, the limit of the increment is

$$\lim_{H_p\to\infty}|\hat{\Phi}(H_p+1,t)-\hat{\Phi}(H_p,t)|=0 \tag{32}$$

Thus, the absolute value of the gain increment is increasing monotonically as $H_p$ is increased toward a limit which can be calculated using the property

$$\lambda[\mathcal{P}(\mathbf{A})]=\mathcal{P}(\lambda[\mathbf{A}]) \tag{33}$$

where the shorthand notation $\lambda[\mathbf{A}]$ means "the eigenvalues of $\mathbf{A}$", and $\mathcal{P}$ is a polynom. Since $\mathbf{A}$ has one eigenvalue $a$ with multiplicity $N$, it can be concluded that $\sum_{i=1}^{H_p}\mathbf{A}^{H_p-i}$ also has one eigenvalue of multiplicity $N$ given by

$$\lambda\left[\sum_{i=1}^{H_p}\mathbf{A}^{H_p-i}\right]=\sum_{i=10}^{H_p}a^{H_p-i}=\frac{a^{H_p}-1}{a-1} \tag{34}$$

Thus, the limit of the norm of the gain can be bounded

$$\lim_{H_p\to\infty}\|\hat{\Phi}(H_p,t)\|\le\lim_{H_p\to\infty}\frac{a^{H_p}-1}{a-1}\|\hat{\mathbf{C}}^T(t)\|\|\mathbf{B}\| \tag{35}$$

Therefore, it can be concluded that

$$|\hat{\mathbf{C}}(t)^T\mathbf{B}|\le\hat{\Phi}(H_p,t)\le\frac{1}{1-a}\|\hat{\mathbf{C}}(t)^T\|\|\mathbf{B}\| \tag{36}$$

To apply Lemma 1, let $\mathcal{A}(t)=\mathbf{A}-\hat{\Phi}(t)^{-1}\mathbf{B}\hat{\mathbf{C}}(t)^T\mathbf{A}^{H_p}$ and $\mathbf{v}(t)=\mathbf{B}\hat{\Phi}(t)^{-1}u(t)$. If $|\hat{\mathbf{C}}(t)^T\mathbf{B}|>0$, an upper bound of the norm of matrix $\mathcal{A}$ can be evaluated by

$$\begin{aligned}\|\mathcal{A}\|^2&\le\|\mathbf{A}\|^2+|\Phi(t)|^{-2}\|\mathbf{B}\hat{\mathbf{C}}^T(t)\|^2\|\mathbf{A}^{H_p}\|^2\\&\le\|\mathbf{A}\|^2+|\hat{\mathbf{C}}(t)^T\mathbf{B}|^{-2}\|\mathbf{B}\hat{\mathbf{C}}^T(t)\|^2\|\mathbf{A}^{H_p}\|^2\end{aligned} \tag{37}$$

The rank of $\mathbf{B}\hat{\mathbf{C}}^T$ is one, its column space is supported by the vector $\mathbf{B}$ and the corresponding eigenvalue is $\hat{\mathbf{C}}^T(t)\mathbf{B}$. We consider the case where $\hat{\mathbf{C}}^T(t)\mathbf{B}\neq 0$. Then, there exist a transformation matrix $\mathbf{M}(t)=[\mathbf{B}|\mathbf{C}_1(t)^\perp|\dots|\mathbf{C}_{N-1}(t)^\perp]$ ($\mathbf{C}_i(t)^\perp$ are the columns vectors forming a basis spanning the subspace orthogonal to $\hat{\mathbf{C}}$). $\mathbf{M}(t)$ having full rank, it is invertible and $\mathbf{B}\hat{\mathbf{C}}(t)^T=\mathbf{M}(t)\mathbf{Z}(t)\mathbf{M}^{-1}(t)$. $\mathbf{Z}(t)$ is a matrix which entries are all nil except for the first one which is equal to $\hat{\mathbf{C}}^T(t)\mathbf{B}$. It follows that $\mathbf{z}=(1/\hat{\mathbf{C}}^T(t)\mathbf{B})\mathbf{Z}(t)$ is a constant matrix with the first entry equals to one the others being nil. Thus, an upper bound for $\|\mathcal{A}(t)\|^2$ is

$$\|\mathcal{A}(t)\|\le|a+\xi|+\|\mathbf{M}(t)\mathbf{z}\mathbf{M}(t)^{-1}\||a+\xi|^{H_p} \tag{38}$$

$\|\mathbf{M}(t)\mathbf{z}\mathbf{M}(t)^{-1}\|$ is finite and choosing $|\xi|<1-|a|$, it can then be concluded that there exists a value $H_p$ such that the expression at the right hand side of the inequality is less than one.

Since there exists a norm for which $\|\mathcal{A}(t)\|<1$, $\mathcal{A}(t)$ has its eigenvalues within the unit circle, and the two first requirements of the lemma are met. The third requirement is also satisfied due to one of the property of the identification algorithm namely $\lim_{t\to\infty}\hat{\mathbf{C}}^T=\hat{\mathbf{C}}_\infty$.

Finally, the input $u(t)$ and $\hat{\Phi}$ are bounded, it therefore implies that $\|\mathbf{v}(t)\|^2$ is bounded from above as long as $\hat{\mathbf{C}}(t)^T\mathbf{B}\neq 0$.

In the case $r>0$, this later requirement can be relaxed. Because $\hat{\Phi}(t)/(\hat{\Phi}^2(t)+r)<\hat{\Phi}^{-1}(t)$, it can be concluded that the discussed results on the existence of a prediction horizon ensuring stability and the boundedness of the state remain valid.

In the particular case of a step input, when $\hat{\mathbf{C}}$ has reached steady state, it can be concluded from Eq. (25) that $\mathbf{l}(t)$ will reach a constant steady state.

### 3.4. Tracking error

The tracking error can be studied considering the truncated projection of the system (23) provided that $N$ is large enough. For $r=0$, the tracking error is defined by

$$v(t+1)=y_r(t+1)-\mathbf{C}^T\mathbf{l}_\mathbf{s}(t+1) \tag{39}$$

Introducing the dynamic equation leads to

$$v(t+1)=y_r(t+1)-\mathbf{C}^T(\mathbf{A}\mathbf{l}_\mathbf{s}(t)+\mathbf{B}v(t)) \tag{40}$$

Noticing that the controller can actually be written using the tracking error

$$v(t+1)=y_r(t+1)-\mathbf{C}^T[\mathbf{A}\mathbf{l}_s(t)+\mathbf{B}\hat{\Phi}^{-1}(t)(v(t)-\hat{\Psi}(t)\mathbf{l}(t))] \tag{41}$$

Introducing $v(t)-y_r(t)+\mathbf{C}^T\mathbf{l}_\mathbf{s}(t)=0$ at the right hand side of the equality, gives after some algebra

$$\begin{aligned}v(t+1)=(1-\mathbf{C}^\mathbf{T}\mathbf{B}\hat{\Phi}^{-1}(t))v(t)+\Delta y_r(t)\\+\mathbf{C}^T[(\mathbb{I}-\mathbf{A})\mathbf{l}_\mathbf{s}(t)+\mathbf{B}\hat{\Phi}^{-1}(t)\hat{\Psi}(t)\mathbf{l}(t)]\end{aligned} \tag{42}$$

with $\Delta y_r(t)=y_r(t+1)-y_r(t)$. $\mathbf{S}$ verifies the identity

$$\mathbf{S}=(\mathbf{A}-\mathbb{I})^{-1}(\mathbf{A}^{H_p}-\mathbb{I})=(\mathbf{A}^{H_p}-\mathbb{I})(\mathbf{A}-\mathbb{I})^{-1} \tag{43}$$

and since $\mathbf{l}_\mathbf{s}(t)=\mathbf{l}(t)$ after the transient of the state error, Eq. (42) writes

$$v(t+1)=(1-\mathbf{C}^\mathbf{T}\mathbf{B}\hat{\Phi}^{-1}(t))v(t)+\Delta y_r(t)-\mathbf{C}^T\left[\mathbb{I}-\frac{\mathbf{B}\mathbf{C}_\mathbf{m}^T\mathbf{S}}{\mathbf{C}_\mathbf{m}^T\mathbf{S}\mathbf{B}}\right](\mathbf{A}-\mathbb{I})\mathbf{l}(t) \tag{44}$$

The factor $1-\mathbf{C}^\mathbf{T}\mathbf{B}\hat{\Phi}^{-1}(t)$ must lie within the interval $]-1,1[$ for asymptotic stability of the tracking error. Let $\mathbf{\Delta C}$ be the identified weight error vector such that $\mathbf{C}-\hat{\mathbf{C}}=\mathbf{\Delta C}$ then the following conditions ensure this requirement:

$$\frac{\mathbf{C}^T\mathbf{B}}{\hat{\mathbf{C}}^T\mathbf{S}\mathbf{B}}>0 \tag{45}$$

$$|\mathbf{\Delta C}^T\mathbf{B}|<|\hat{\mathbf{C}}^T(2\mathbf{S}-\mathbb{I})\mathbf{B}| \tag{46}$$

The matrix $\mathbf{S}$ is positive, therefore condition (45) states that the weights of the actual system and the identified one should lie within the same half space delimited by the orthogonal subspace of $\mathbf{B}$. Noting that the static gain of the system $\mathbf{C}^T(\mathbb{I}-\mathbf{A})^{-1}\mathbf{B}$ has the same sign as $\mathbf{C}^T\mathbf{B}$, this finally indicates that the sign of the static gains of the system and its model should be the same.

Condition (46) relates the modeling error to the model. Conservative relationship can be proposed depending on the sign of $a$

$$\begin{cases}|\mathbf{\Delta C}^T\mathbf{B}|<|\hat{\mathbf{C}}^T\mathbf{B}| & \text{if } a>0\\ |\mathbf{\Delta C}^T\mathbf{B}|<\dfrac{1+a-2a^{H_p}}{1-a}|\hat{\mathbf{C}}^T\mathbf{B}| & \text{if } a<0\end{cases} \tag{47}$$

If the conditions are met, it follows from the boundedness of $\mathbf{l}(t)$ and of the reference that the tracking error is bounded.

Recognizing that $\mathbf{B}\mathbf{C}_\mathbf{m}^T\mathbf{S}/\mathbf{C}_\mathbf{m}^T\mathbf{S}\mathbf{B}$ defines the oblique projection on $\mathbf{B}$ along the direction $\ker(\mathbf{S}^T\mathbf{C}_\mathbf{m})$, it follows that $\mathbf{P}_{\mathbf{C}_\mathbf{m}^\perp}=\mathbb{I}-\mathbf{B}\mathbf{C}_\mathbf{m}^T\mathbf{S}/\mathbf{C}_\mathbf{m}^T\mathbf{S}\mathbf{B}$ is the oblique projection on $\mathbf{C}_\mathbf{m}^\perp$ the orthogonal subspace of $\mathbf{C}_\mathbf{m}$ along direction $\mathbf{B}$. Its null space is thus supported by $\mathbf{B}$. In order to simplify Eq. (44) using this property, the dynamic of $\mathbf{l}(t)$ is introduced i.e. $(\mathbf{A}-\mathbb{I})\mathbf{l}(t)=\mathbf{l}(t+1)-\mathbf{l}(t)-\mathbf{B}u(t)$. The tracking error then writes

$$v(t+1)=(1-\mathbf{C}^\mathbf{T}\mathbf{B}\hat{\Phi}^{-1}(t))v(t)+\Delta y_r(t)-\mathbf{C}^T\mathbf{P}_{\mathbf{C}_\mathbf{m}^\perp}(\mathbf{l}(t+1)-\mathbf{l}(t)) \tag{48}$$

In the case of a step reference, this latest expression shows that as the state vector reaches a steady state, the tracking error vanishes to zero and does not depend on the accuracy of the model.



Please cite this article as: Kannan S, et al. Application of Laguerre based adaptive predictive control to Shape Memory Alloy (SMA) Actuator. ISA Transactions (2013), http://dx.doi.org/10.1016/j.isatra.2013.02.004

The effect of an additive noise on the measurement is now considered. Replacing $v(t)$ by $v(t)+n(t)$ (where $n(t)$ is the noise model supposed have zero mean) in (40) and following the same lines, the previous equation is modified as follows:

$$v(t+1) = (1-\mathbf{C^T B}\hat{\Phi}^{-1}(t))v(t)+\Delta y_r(t) \\ -\mathbf{C}^T\mathbf{P}_{\mathbf{C_m^\perp}}(\mathbf{l}(t+1)-\mathbf{l}(t))+\mathbf{C^T B}\hat{\Phi}^{-1}(t)n(t) \quad (49)$$

thus, under the same assumptions, the mean tracking error is equal to zero in steady state.

This property is not conserved when $r>0$. This is easily shown by replacing $\hat{\Phi}(t)$ by $\hat{\Phi}(t)/(\hat{\Phi}^2(t)+r)$ and following the same lines to obtain the expression of $v(t)$. It follows that the expression becomes:

$$v(t+1) = \left(1-\mathbf{C^T B}\frac{\hat{\Phi}(t)}{\hat{\Phi}^2(t)+r}\right)v(t)+\Delta y_r(t) \\ -\frac{\hat{\Phi}^2(t)}{\hat{\Phi}^2(t)+r}\mathbf{C}^T\mathbf{P}_{\mathbf{C_m^\perp}}(\mathbf{l}(t+1)-\mathbf{l}(t)) \\ -\frac{r}{\hat{\Phi}^2(t)+r}\mathbf{C}^T(\mathbf{A}-\mathbb{I})\mathbf{l}(t) \quad (50)$$

First the pole of the tracking error will be modified, its limit tending to 1 as $r$ is increased (for a given $\hat{\Phi}(t)$). Moreover, as $\mathbf{l}(t)$ reaches a steady state, the input term no longer vanishes. This is consistent with the fact $r$ was introduced to control the trade-off between tracking precision and control effort.

## 4. Experimental assessment

### 4.1. Experimental setup

The setup schematic is depicted in Fig. 3(a) and a picture of the test bench in Fig. 3(b). It uses a NitiNol SMA wire to produce linear displacement a simple yet usual configuration [26,27,7]. Its dimension are 21 cm in length and 200 μm in diameter. Austenite start temperature is 65 °C and austenite finish temperature is 93 °C. The measured resistance at room temperature is 8 Ω. A constant stress of 87 MPa is applied using a weight of 280 g. The actuation is kept within 2% strain resulting in a theoretical travelling range of 4.2 mm. Fig. 4 shows the hysteresis of the actuator. A larger displacement is actually obtained in practice.

The ambient temperature is not controlled, the wire is cooled by natural convection. A theoretical estimate of the cooling time would be comprised between 10 s and 40 s depending on the estimated value of convection coefficient considered. These values are consistent with the ones measured experimentally.

The power supply is build around L165H operational amplifier which provides voltage amplification and sufficient power capability. The voltage is kept between 0 and 3 V corresponding to a maximum current of ca 0.4 A to prevent deterioration of the wire through excessive heating. Consequently the maximum heating power can be evaluated to be less than 1.5 W. Current, and thus heating power, is not directly measured.

Apart from voltage, the displacement is measured by a laser sensor (Waycon LAS-TM-10) pointing toward the payload. The control was implemented and tested using a DSpace 1104 card. Sampling frequency is 1 kHz.

### 4.2. Test protocol

Influence of the order of the filter, of the prediction horizon and of the weighting factor $r$ were experimentally evaluated. Table 1 sums up the parameter kept constant. A unique variable step signal was applied for all tests, to ensure replication of the sequences of major and minor loops of the hysteresis curve and to perform analysis on the displacement tracking results.

The criterion selected were the overshoot (%), settling time (s), steady state error (%) and oscillations (%) which occur at every step change in the reference signal. Tests were repeated and means of the different performance criteria were calculated from measurements at each step change of the reference signal.

### 4.3. Influence of r

The results of the tests are summed up in Table 2 where the abbreviation MO, MST, MSSE, MOS stand for mean overshoot, mean settling time, mean steady state error and mean oscillations. As expected, the controller achieves the reference if $r=0$. The transient degrades with the increase of $H_p$: settling time is of

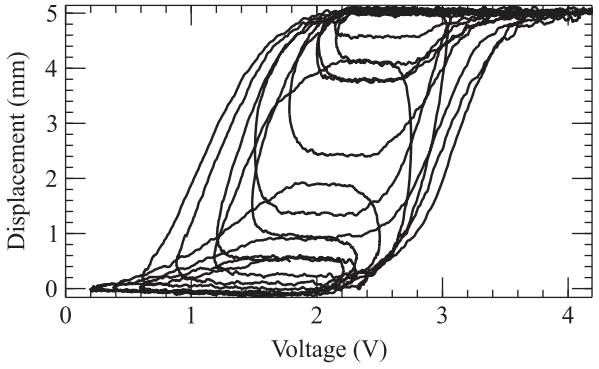


**Fig. 4.** Hysteresis of the actuator used in the experiment.

**Table 1**
Constant parameters during the tests.

| Pole | Initialization | Threshold | Forgetting factor |
|---|---|---|---|
| $a=0.9$ | $P(0)=1\times10^5\mathbb{I}$ | $\eta=1\times10^{-3}$ | $\lambda=0.5$ |

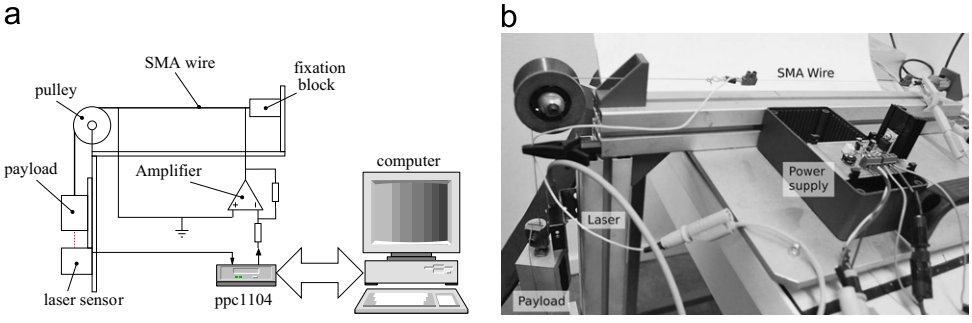


**Fig. 3.** Experimental setup: schematic (a) and picture of the setup (b).



Please cite this article as: Kannan S, et al. Application of Laguerre based adaptive predictive control to Shape Memory Alloy (SMA) Actuator. ISA Transactions (2013), http://dx.doi.org/10.1016/j.isatra.2013.02.004

**Table 2**
Evaluation criteria for the adaptive predictive control. The entries resulting in instability are signaled by the "n.a" abbreviation.

| $H_p$ | Criteria | $r=10^{-2}$ | $r=10^{-4}$ | $r=0$ |
|---|---|---|---|---|
| 30 | MO | 0.8 | 15.0 | 14.2 |
| | MST | 12.8 | 16.0 | 22.5 |
| | MSSE | 34.2 | 11.7 | 0.0 |
| | MOS | 1.4 | 14.6 | 14.4 |
| 15 | MO | n.a | 7.6 | 4.7 |
| | MST | | 12.7 | 11.0 |
| | MSSE | | 0.0 | 0.0 |
| | MOS | | 5.9 | 8.7 |
| 3 | MO | n.a | 3.7 | 0.7 |
| | MST | | 8.3 | 5.3 |
| | MSSE | | 6.8 | 0.0 |
| | MOS | | 0.0 | 0.5 |

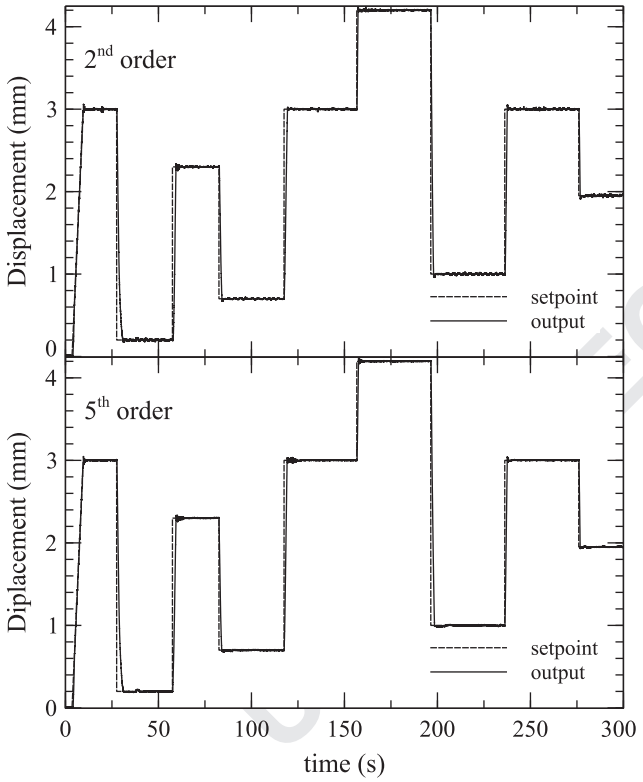


**Fig. 5.** Outputs of the controlled SMA actuator for 2nd and 5th order filters respectively ($H_p=3$, $r=0$).

course expected to increase, but unfortunately the overshoot follows the same trend. The parameter $r$ reduces the control activity. Consequently, the identification will perform less effectively as the frequency content of the control signal becomes poorer. This results in larger steady state error. Too large values of $r$ cause the system to diverge although initially introduced to prevent instabilities due to the vanishing of $\hat{\Phi}(t)$. However, as already revealed by Eq. (50), $r$ can also have a destabilising effect. It appears that leaving $r=0$ is actually best since no instabilities were observed, and the mean steady state error is nil.

### 4.4. Influence of the filter order

Two filters respectively of 2nd and 5th order were tested. Reducing the truncation order will affect the accuracy of the model because the approximation of the transfer function becomes less precise for high frequencies, and bias is introduced in the identified coefficients. The tracking performances (Figs. 5–7, top: 2nd order, bottom 5th order) are however very similar.

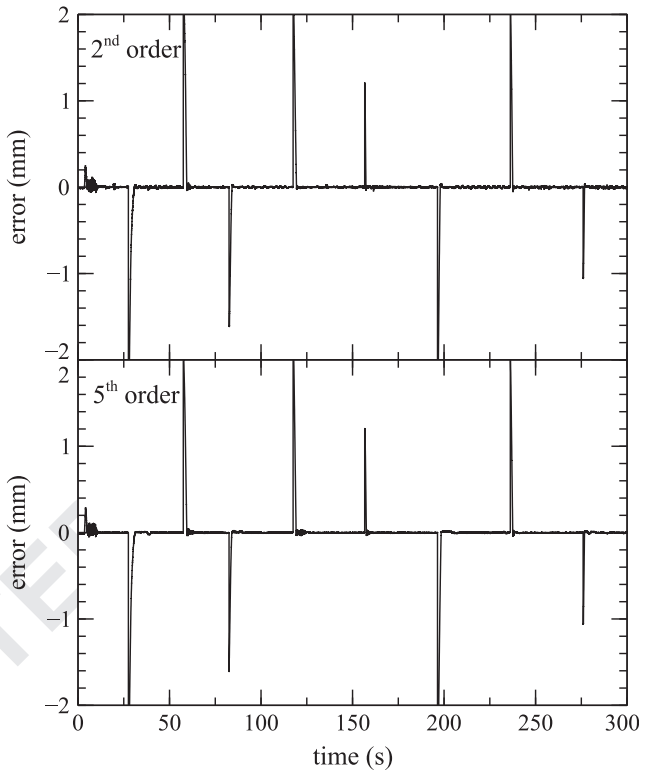


**Fig. 6.** Tracking errors of the controlled SMA actuator for 2nd and 5th order filters respectively ($H_p=3$, $r=0$).

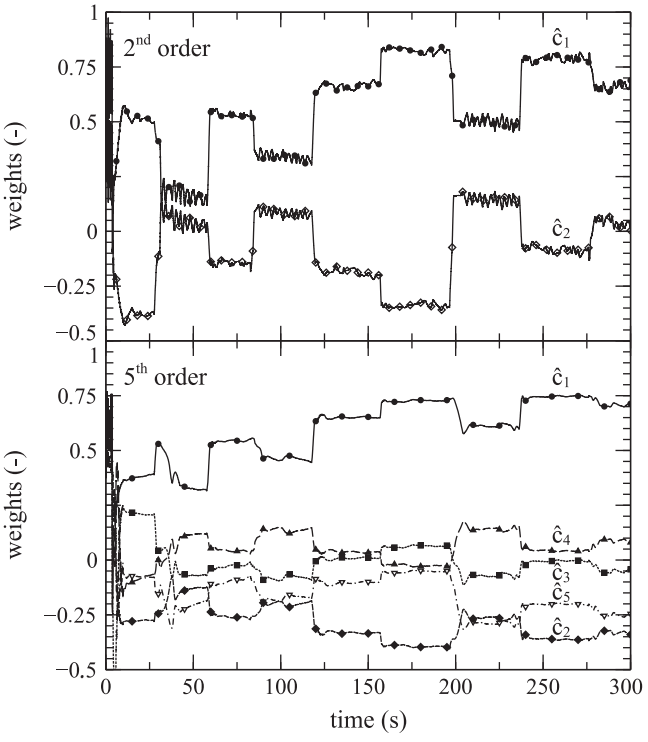


**Fig. 7.** Identified weights of the SMA actuator for 2nd and 5th order filters respectively ($H_p=3$, $r=0$) in closed loop.

Please cite this article as: Kannan S, et al. Application of Laguerre based adaptive predictive control to Shape Memory Alloy (SMA) Actuator. ISA Transactions (2013), http://dx.doi.org/10.1016/j.isatra.2013.02.004

In both case the identification is working properly, the errors being zero mean white noise signals with a larger variance in the case of the 2nd order (approximately 0.01 vs $1 \times 10^{-3}$ for the fifth order). However, the filter weights $\hat{c}_0$ and $\hat{c}_1$ are different for the two models (Fig. 7). Despite the difference of the models, the closed loop output is virtually unchanged, proving that the tracking error is robust to the modeling error as discussed in Section 3.4 (Fig. 6).

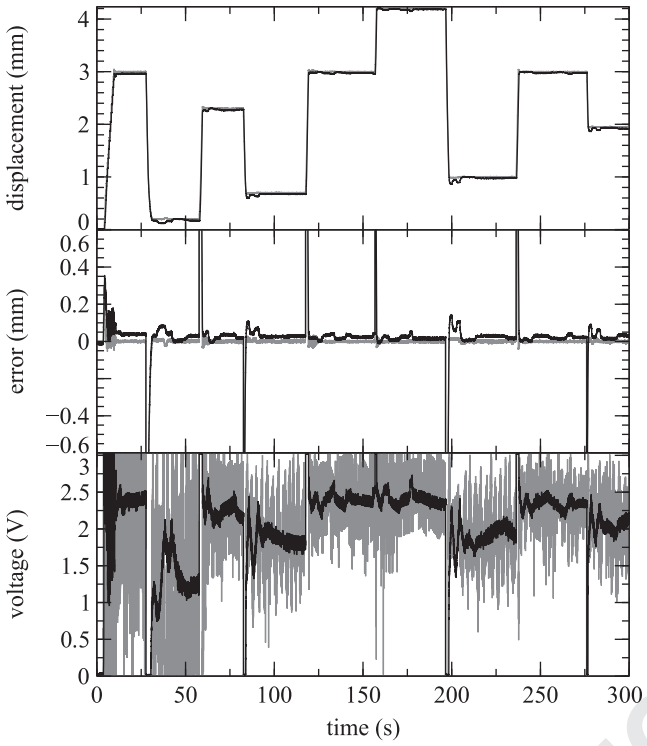


**Fig. 8.** Effects of the prediction horizon for $H_p=3$ (gray curves) and $H_p=30$ (black curves) on the outputs (top), tracking errors (middle) and control signals (bottom). $r=0$ for these tests.

### 4.5. Prediction horizon

The prediction horizon $H_p$ acts directly on the controller signal. Fig. 8 (from top to bottom: outputs, tracking errors and control signals) shows the results for two prediction horizon $H_p=3$ and $H_p=30$. As the prediction horizon increases the transient is degraded: this is clearly visible on the tracking error. The signal gets smoother and the tracking performance degrade in steady state (see Table 2). This can be explained by a poorer input for the identification whereas the model must predict the dynamic on a longer horizon.

### 4.6. Disturbances rejection

Disturbances were obtained by blowing air toward the wire. Fig. 9 shows their effects on the output in the case were $r=0$ (top) and $r=1 \times 10^{-4}$ (bottom). In both case the controller reacts by applying the maximum voltage available (Fig. 10). For $r=0$, the chattered control signal induces fluctuation of the output from $t=143$ s to $t=146$ s (Fig. 10). Note that this exaggerated control activity is due to the low prediction horizon ($H_p=3$) set for this experiment. This is corrected by increasing $r$ at the price of slightly less precision at steady state (Fig. 9). It can also be observed that although saturation occurs during the transient and the application of the disturbance, there is no wind-up effect as for proportional–integral correctors.

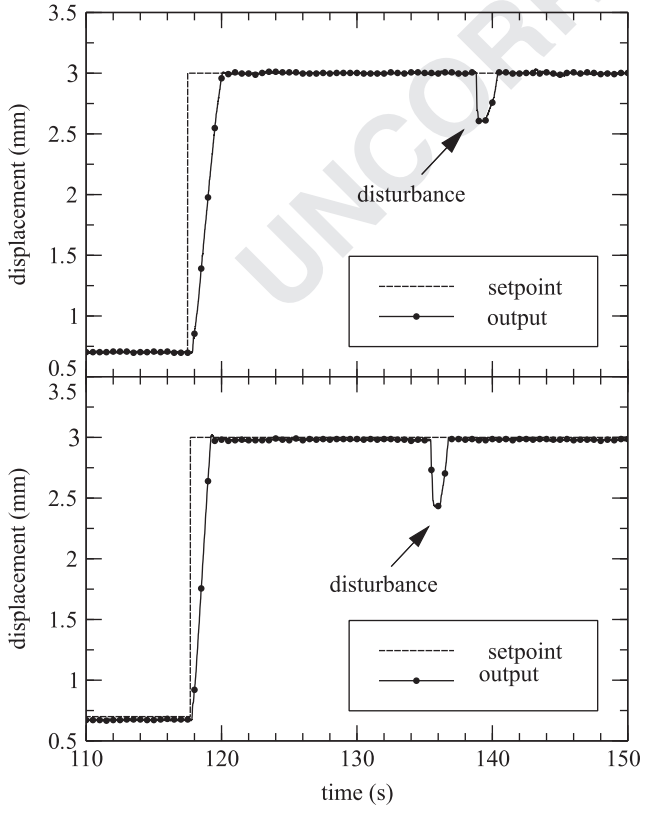


**Fig. 9.** Effect of thermal disturbance on the outputs for $r=0$ and $r=1 \times 10^{-4}$ respectively ($H_p=3$, $N=5$).

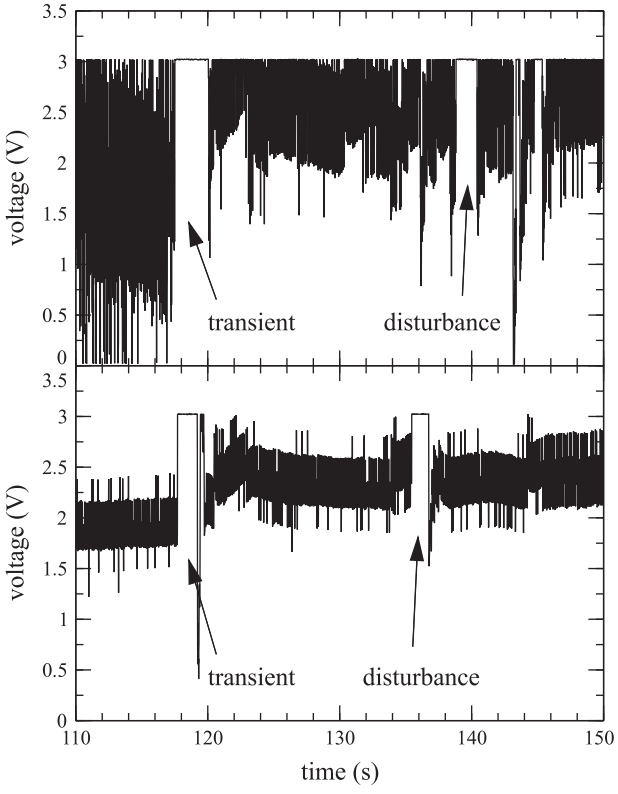


**Fig. 10.** Effect of thermal disturbance on the control signals for $r=0$ and $r=1 \times 10^{-4}$ respectively ($H_p=3$, $N=5$).



Please cite this article as: Kannan S, et al. Application of Laguerre based adaptive predictive control to Shape Memory Alloy (SMA) Actuator. ISA Transactions (2013), http://dx.doi.org/10.1016/j.isatra.2013.02.004

### 4.7. Identification algorithm

To illustrate the benefits of the chosen identification algorithm, tests were also performed implementing a standard exponential forgetting factor algorithm (forgetting factor set to 0.99). Results can be seen in Fig. 11 and can be compared to those of Fig. 5. They clearly show typical intermittent bursting of the weights (Fig. 11, bottom). It is remarkable though that the system remains stable and still reach the setpoint once the bursting has vanished.

### 4.8. Application to an antagonistic set-up

The stress applied to actuator studied so far is due to the pay load which was chosen to ensure optimal pre-stress. This is a special case where a non-linear hysteretic relation exists between strain and temperature.

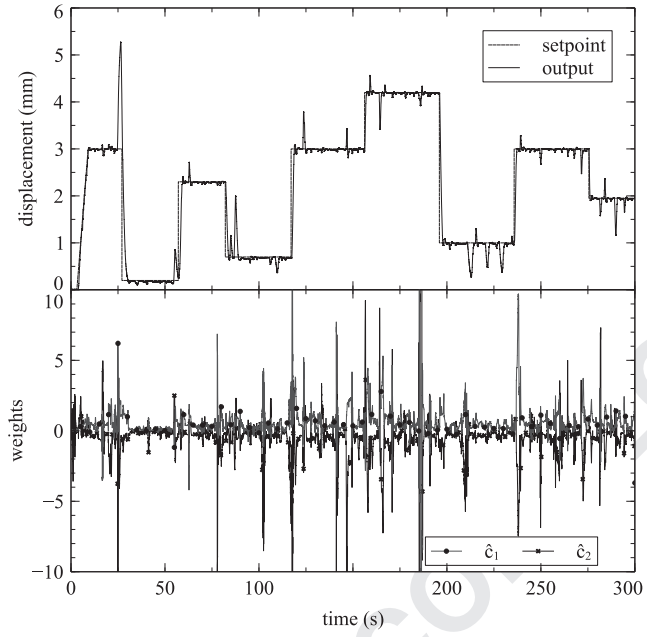


**Fig. 11.** Output of the controlled SMA actuator for the 2nd order filters ($H_p$=3, $r$=0) with forgetting factor equal to 0.99.

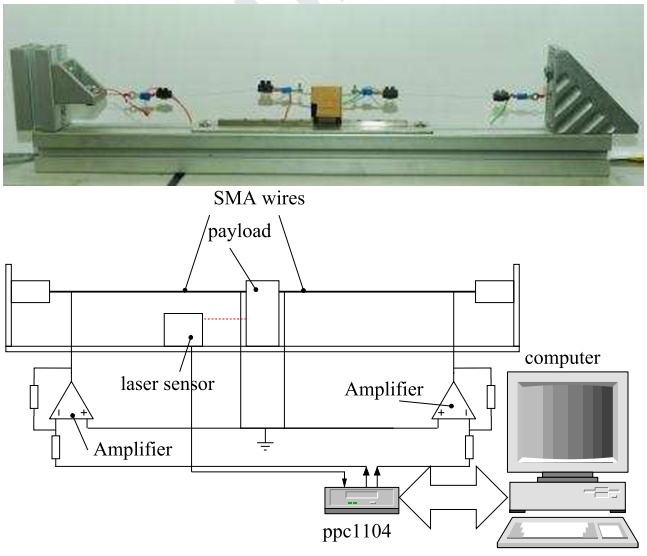


**Fig. 12.** Picture of the antagonistic actuator set-up (the wires are 200 μm in diameter and are almost invisible), and schematic of the set-up.

Generally, in SMA the hysteresis relates strain, stress and temperature. In this section, the controller is applied to a so called antagonist actuator, where two SMA wires are used and arranged as represented in Fig. 12. The wires are elongated to obtain an initial pre-strain of roughly 2%. Wires are heated independently. A heated wire recover the initial strain. This will result in the displacement in one direction of the payload, and at the same time will increase the strain in the opposite wire (thus reaching a cumulated strain up to 4%).

The advantage offered by this type of actuator is that it is no longer under actuated in the sense that for both directions the dynamic is imposed by the heating power (in the previous actuator, the dynamic was imposed by the thermal time constant of the wire during cooling). On the other hand, temperature in the wire build up rapidly if the wire is heated too often, because the cooling time between two actuation of the same wire might not long enough. The stress in the wires will therefore increase.

On the schematic of Fig. 12, the power is supplied by two separate amplifiers. The power is split according to the sign of the controller output e.g if the later is negative the corresponding voltage is applied to the left wire and vice-versa. From the control point of view, the system remains single input, single output, and the previous controller may be used. However, the hysteresis is more complex (see Fig. 13), and the stress varies constantly for the reasons already discussed. A bias on the displacement is also visible. The only measurements available are the displacement and the voltages (Fig. 12).

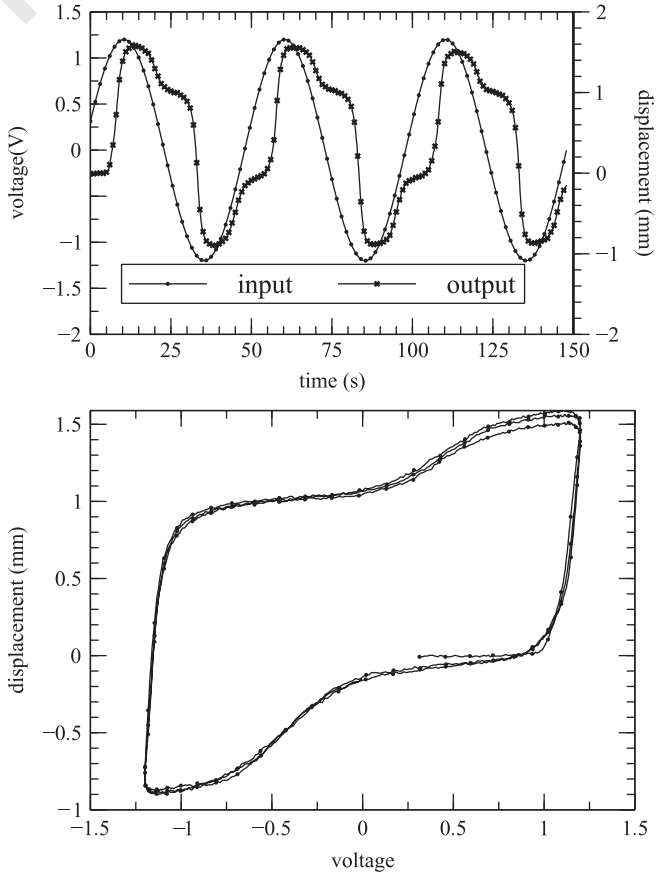


**Fig. 13.** A sinusoidal reference is applied resulting in alternative heating of the wires. Note that, for the sake of simplicity, the voltages applied to each wire have been merged on the figure (top). Actually, the wires on which the voltages are applied are selected according to the sign of the reference. Effect of the hysteresis of the antagonist actuator for an input describing an internal loop are depicted on the bottom figure.



Please cite this article as: Kannan S, et al. Application of Laguerre based adaptive predictive control to Shape Memory Alloy (SMA) Actuator. ISA Transactions (2013), http://dx.doi.org/10.1016/j.isatra.2013.02.004

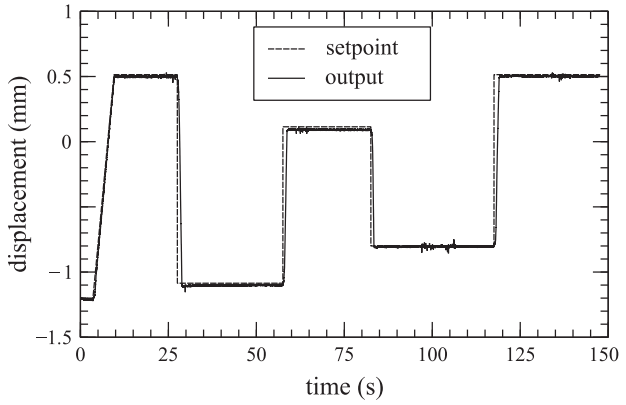


**Fig. 14.** Output of the antagonistic actuator for a 2nd order filter ($H_p$=3, $r$=0).

Fig. 14 shows the result of the tracking of a reference similar to the one used for the single actuator, although scaled and shifted to ensure that both wires are activated during the test. The filter used is a second order and the prediction horizon is set to 3. From the result obtained, it can be concluded that the controller is still working correctly.

## 5. Discussion and conclusion

### 5.1. Main results

In this paper, an adaptive predictive controller based on Laguerre rational basis functions has been used to control SMA actuators. The properties of the controller proposed in [14,28] have been studied using different tools. This led to the following results:

- stability of the state is related to the choice of the prediction horizon $H_p$ and convergence of the identification;
- if some conditions on the modelling error are verified, the tracking error is asymptotically stable and vanishes in the case of a step input *independently of modeling error*.

This is a general result which explains the robustness of the controller. It is of particular interest for the application addressed here, where the non-linearity can influence the accuracy of the weights identified.

An interesting experimental observation is that the saturation implemented to protect the SMA wire did not influence the stability of the control. This is an advantage over a PI controller which would necessitate an anti-windup mechanism.

The weighting of the control signal introduced to provide a tuning parameter was not satisfactory. It does help to immunize the system against the room temperature variation for setting point near the limits of the supply, but the poorer steady state precision and the instabilities appearing are not acceptable.

### 5.2. Discussion

The control of SMA actuators has been addressed a lot in literature. Although not new, the controller proposed by Dumont presents some properties that this paper has revealed. We sum up briefly its advantages compared to some other adaptive or adaptive predictive control strategies.

First, The Laguerre filters have a very simple known structure, hence the design is straightforward. The accuracy of the model is directly linked to the order of the truncation and converge monotonically toward the best approximation. Moreover, the truncation order of the Laguerre filter can be optimized by a proper choice of $a$. By contrast, there are no such properties for neural networks or fuzzy controllers: their complexity increases exponentially with precision [29,30], and the approximation error is discontinuous [31].

Compared to standard adaptive predictive controllers, using Laguerre filters reduces the number of parameters to be identified, and no pole/zero cancellations are possible. In [32], the ARMA model proposed requires nine parameters, to be compared to a maximum order of five in the present study. Moreover, no Diophantine equations must solved on-line for the controller studied.

Orthogonal basis functions applied to adaptive model predictive control (AMPC) has also been studied. In [33], a Laguerre incremental model and an AMPC are proposed. Following the usual methods of generalized MPC, the controller therefore depends on the calculation of matrices (dimensions: prediction horizon times control horizon) and their inverse at each time steps. These calculations are not needed in the case of the controller used.

To temper these remarks, it must be added that these results were possible because the sampling rate is still much faster than the natural time response of the actuators studied. Moreover, the on-line identification is critical. The algorithm proposed by [22] has been used to guarantee the boundedness of the information matrix. However, in some cases when $H_p$ is large, the control activity is not persistently exciting. The identified weights then tend to become large (but bounded). This results in degraded transient performances.

### 5.3. Conclusion

The initial goals of this paper were to design a simplified adaptive controller in order to control SMA actuators, measuring only displacement. Another requirement was to avoid any training or offline identification for the tuning of the controller. To this end, an association of a simple adaptive predictive controller using a Laguerre [14] and a directional forgetting RLS algorithm was proposed. The expected advantages have been theoretically studied and the robustness with respect to modelling error has been proven. The experimental results confirm the effectiveness of the control.

Chatter appears in the voltage for low values of $H_p$. This is not an issue as far as the SMA is concerned. For the analog power supply, this is not desirable, hence in the future a switched power supply will be used. Further improvements should address the on-line identification and ensure that the conditions for stability and convergence of the tracking error are respected.

## References

[1] Patoor E, Lagoudas DC, Entchev PB, Brinson LC, Gao X. Shape memory alloys part I: general properties and modeling of single crystals. Mechanics of Materials 2006;38(5–6):391–429.
[2] Kuwano N, Wayman C. Some effects of parent phase aging on the martensitic transformation in a Cu–Al–Ni shape memory alloy. Metallurgical and Materials Transactions A 1984;15(4):621–6.
[3] Nespoli A, Besseghini S, Pittaccio S, Villa E, Viscuso S. The high potential of shape memory alloys in developing miniature mechanical devices: a review on shape memory alloy mini-actuators. Sensors and Actuators A: Physical 2010;158(1):149–60.
[4] Mrad RB, Hu H. A model for voltage-to-displacement dynamics in piezoceramic actuators subject to dynamic-voltage excitations. IEEE/ASME Transactions on Mechatronics 2002;7(4):479–89.
[5] Tan X, Baras JS. Adaptive identification and control of hysteresis in smart materials. IEEE Transactions on Automatic Control 2005;50(6):827–39.



Please cite this article as: Kannan S, et al. Application of Laguerre based adaptive predictive control to Shape Memory Alloy (SMA) Actuator. ISA Transactions (2013), http://dx.doi.org/10.1016/j.isatra.2013.02.004

[6] Benzaoui H, Chaillet N, Lexcellent C, Bourjault A. Nonlinear motion and shape control of shape memory alloy. In: Proceedings of the SPIE symposium on smart structures and materials; 1999. p. 337–48.
[7] Elahinia MH, Ahmadian M. Application of the extended Kalman filter to control of a shape memory alloy arm. Smart Materials and Structures 2006;15:1370.
[8] Webb GV, Lagoudas DC, Kurdila AJ. Hysteresis modeling of SMA actuators for control applications. Journal of Intelligent Materials, Systems and Structures 1998;9(6):432–48.
[9] Kuhnen K. Modeling, identification and compensation of complex hysteretic nonlinearities. A modified Prandtl–Ishlinskii approach. European Journal of Control 2003;9(4):407–18.
[10] Iyer RV, Tan X, Krishnaprasad PS. Approximate inversion of the Preisach hysteresis operator with application to control of smart actuators. IEEE Transactions on Automatic Control 2005;50(6):798–810.
[11] Janocha H, Kuhnen K. Realtime compensation of hysteresis and creep in piezoelectric actuators. Sensors and Actuators 2000;79(2):83–9.
[12] Asua E, Etxebarria V, Garcí a-Arribas A. Neural network-based micropositioning control of smart shape memory alloy actuators. Engineering Applications of Artificial Intelligence 2008;21:796–804.
[13] Ma N, Song G, Lee H. Position control of shape memory alloy actuators with internal electrical resistance feedback using neural networks. Smart Materials and Structures 2004;13:777–83.
[14] Zervos CC, Dumont G. Deterministic adaptive control based on Laguerre series representation. International Journal of Control 1988;48(6):2333–59.
[15] Reynaerts D, Brussel HV. Design aspects of shape memory actuators. Mechatronics 1998;8(6):635–56.
[16] Wahlberg B. System identification using Laguerre models. IEEE Transactions on Automatic Control 1991;36(5):551–62.
[17] Hoff PMJVD, Heuberger PSC, Bokor J. System identification with generalized orthonormal basis functions. Automatica 1995;31(12):1821–34.
[18] Ninness B, Gibson S, Weller S. Practical aspects of using orthonormal system parameterisations in estimation problems. In: Proceedings of the 12th IFAC symposium on system identification, vol. 2. Citeseer; 2000. p. 463–8.
[19] Oliveira e Silva T. Optimality conditions for truncated Laguerre networks. IEEE Transactions on Signal Processing 1994;42(September (9)):2528–30.
[20] Bouzrara K, Garna T, Ragot J, Messaoud H. Decomposition of an ARX model on Laguerre orthonormal bases. ISA Transactions 2012;6(November):848–60.
[21] Wang L. Discrete time model predictive control design using Laguerre functions. In: American control conference, 2001. Proceedings of the 2001, vol. 3. IEEE; 2001. p. 2430–5.
[22] Cao L, Schwartz H. A directional forgetting factor based on decomposition of information matrix. Automatica 2000;36(11):1725–31.
[23] Dumont GA, Fu Y. Non-linear adaptive control via Laguerre expansion of Volterra kernels. International Journal of Adaptive Control and Signal Processing 1993;7(5):367–82.
[24] Landau YD, Lozano Z, M'saad M, Karimi A. Adaptive control: algorithms, analysis and applications. Communication and control engineering. 2nd ed.Springer; 2011.
[25] Tao G. Adaptive control design and analysis, vol. 37. Wiley-IEEE Press; 2003.
[26] Song G, Ma N. Robust control of a shape memory alloy wire actuated flap. Smart Materials and Structures 2007;16:N51–7.
[27] Price AD, Jnifene A, Naguib HE. Design and control of a shape memory alloy based dexterous robot hand. Smart Materials and Structures 2007;16:1401–14.
[28] Dumont GA, Zervos CC, Pageau GL. Laguerre based adaptive control of pH in an industrial bleach plant extraction stage. Automatica 1990;26(4):781–7.
[29] Kŭrková V. Approximation of functions by perceptron networks with bounded number of hidden units. Neural Networks 1995;8(5):745–50.
[30] Gripenberg G. Approximation by neural networks with a bounded number of nodes at each level. Journal of Approximation Theory 2003;122(June (2)):260–6.
[31] Kainen PC, Kŭrková V, Vogt A. Approximation by neural networks is not continuous. Neurocomputing 1999;29(1):47–56.
[32] Tai NT, Kha NB, Ahn KK. Predictive position and force control for shape memory alloy cylinders. Journal of Mechanical Science and Technology 2010;24(8):1717–28.
[33] Zhang H, Chen Z, Wang Y, Li M, Qin T. Adaptive predictive control algorithm based on Laguerre Functional Model. International Journal of Adaptive Control and Signal Processing 2006;20(March (2)):53–76.



Please cite this article as: Kannan S, et al. Application of Laguerre based adaptive predictive control to Shape Memory Alloy (SMA) Actuator. ISA Transactions (2013), http://dx.doi.org/10.1016/j.isatra.2013.02.004